Scientia Iranica A (2015) 22(1), 15–29

SCIENTIA IRANICA

Sharif University of Technology
Scientia Iranica
Transactions A: Civil Engineering
www.scientiairanica.com

Studying near fault endurance time acceleration function

B. Ghahramanpoor[a,*], N. Fanaie[a] and H. Jahankhah[b]

a. *Department of Civil Engineering, K.N.Toosi University of Technology, Tehran, Iran.*
b. *International Institute of Earthquake Engineering and Seismology, Tehran, Iran.*

Received 12 May 2013; received in revised form 9 February 2014; accepted 5 August 2014

KEYWORDS
Endurance time method;
Near fault earthquakes;
Intensifying acceleration function;
Forward directivity.

Abstract. The Endurance Time (ET) method is a time-history based dynamic pushover procedure. In this method, the structures are subjected to gradually intensifying acceleration called an acceleration function. Then, their performances are assessed from linear to collapse level based on the interval time through which they can satisfy the required objectives. ET Acceleration Functions (ETAFs) are calibrated upon actual earthquake spectra compatible with the Iranian National Building Code (standard no. 2800). In this code, there is no distinction between far and near fault regions. ETAFs scale based spectrum increases uniformly at all periods as the time passes which is why this uniform increment is not desirable in near fault earthquakes. As the rupture propagation is oriented towards a site, near fault earthquakes have further spectral acceleration in the period over 0.6 sec compared to far fault earthquakes. The shape of the spectrum becomes richer over long periods as its level increases. In this research, ETAFs are presented for near fault target spectra, provided by Abrahamson-Silva attenuation relations. These relations have been modified by Somerville near fault correction coefficients. According to the results obtained in this research, while the new acceleration function can model directivity effects at higher periods, it also satisfies endurance time concepts.

1. Introduction

Nowadays, it is very important to properly design and retrofit structures against strong earthquakes. Physical and economical losses, caused by earthquakes in recent decades, has revealed the deficiencies and shortcomings of traditional methods in earthquake resistance design. Therefore, engineers and researchers are seeking new approaches for design and analytical methods. Performance Based Design (PBD) is a new concept in which various performance objectives are satisfied under different ground motions from minor to severe ranges. The Endurance Time (ET) method is the most recent performance based analytical procedure provided and developed by Estekanchi et al. [1], which is basically a simple dynamic pushover procedure. In this method, the damage measures of structures are predicted at different intensity measures by subjecting them to some pre-designed intensifying dynamic excitations called Endurance Time Acceleration Functions (ETAFs). ETAFs are designed in such a way that their intensities increase through time. As the demand of ETAFs increases, the structures gradually go from an elastic to a nonlinear inelastic phase, and finally meet global dynamic instability [1].

Application of the ET method in linear and nonlinear analysis of structures has been proved in comparison with most known analysis methods such

*. *Corresponding author. Tel.: +98 914 1601788; Fax: +98 21 88757802*
E-mail addresses: b.ghahramanpoor@yahoo.com (B. Ghahramanpoor); fanaie@kntu.ac.ir (N. Fanaie); h. jahankhah@iiees.ac.ir (H. Jahankhah)

as Incremental Dynamic Analysis (IDA), and the nonlinear static procedure (pushover method) [1,2].

ETAFs are calibrated based on 7 real earthquakes compatible with the design spectrum of the Iranian National Building Code, corresponding to soil profile type 2. Near fault effects have not been considered in the conventional ETAFs. In this research, ET concepts have been developed for near fault earthquakes due to the importance of such motions.

In ETAFs, each time represents one earthquake level which increases as the time goes up. These functions scale the spectra uniformly at all periods as the time increases; while, in near fault earthquakes the spectrum is relatively richer over long periods as its level increases. So the spectral characteristics of conventional ETAFs are generally different from those of near fault earthquakes.

Near fault earthquakes have intensified spectral acceleration for periods over 0.6 sec [3], compared to far fault ones, due to the forward directivity phenomenon, and rupture propagation towards a site. The increment rate of spectral amplitude rises at longer periods and stronger earthquake levels.

As there are almost no near fault design spectrum in seismic codes, the modified attenuation relationships are usually used in engineering research to consider directivity effects. In this research, first, 5 near fault target spectra have been produced corresponding to 5 moment magnitudes. They have been developed using Abrahamson-Silva (1997) [4] attenuation relations modified by Somerville et al. (1997) [3] near fault coefficients. Then, the frequency content of Gaussian white noise is modified so that the resulting response spectrum matches the target spectrum at predefined target times. As known, intensification of near fault ground motion response spectra in long period regions is a result of the directivity-pulse existence in relative records. From this point of view, correction factors to spectra ordinates for periods more than 0.6 sec reflect the probable existence of such pulses implicitly. However, the generated ground motions based on such corrected spectra may not percontain a single dominant velocity pulse explicitly. Production of the near fault acceleration function has been generally expressed in the following sections. According to the results, the new acceleration functions can properly predict the directivity effects of near fault earthquakes.

2. Endurance time method

The endurance time method is a new dynamic procedure that can predict the seismic performance of structures. In this method, the structures are subjected to a gradually intensifying dynamic excitation and their performances are monitored at different excitation levels. The structures that endure the imposed intensifying acceleration function for a longer time are expected to sustain stronger seismic excitation. In fact, in ET analysis, the time axis can be correlated to excitation intensity because of intensifying acceleration functions [2].

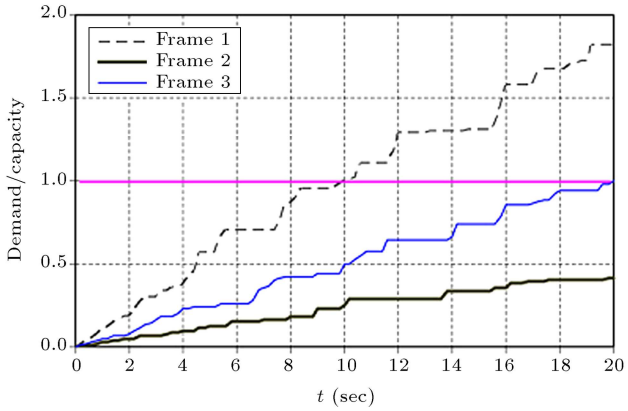

Figure 1. Demand/capacity of frames under acceleration function [1].

The concept of the ET method can be physically presented by a hypothetical shaking table experiment. For this purpose, three different frames with unknown seismic properties are fixed on the table and subjected to an intensifying shaking. One of the frames (frame 1 in Figure 1) fails after a short time and the third one will also collapse as the amplitude of the vibration increases. It is assumed that the same will happen to the second frame also. These three frames can be ranked according to their seismic resistance times, i.e. the time at which the models failed. It should be mentioned that the lateral loads, induced by the shaking table, are somehow corresponded with the earthquake loads. Therefore, the endurance time of each structure can be considered the seismic resistance criterion against intensifying shaking. In this hypothetical analysis, the second frame shows the best performance because of its longer endurance time and, therefore, is the strongest structure. The first one is the worst and the third is somewhere in between the first and second frames [1,5]. The demand/capacity ratios of these frames presented in Figure 1 have been calculated as the maximum absolute values of the endurance index during the time interval of "0.0" to "t". Since a structure collapses, when its demand/capacity ratio exceeds unity, the endurance time for each frame can be easily derived from this figure [5].

In order to start an ET time history analysis, the representative model should be constructed and the proper damage measure and ET accelerogram should be set (Figure 2).

The analysis results are usually presented by a curve in which the maximum absolute value of the damage measured in the time interval [0; t] (as given

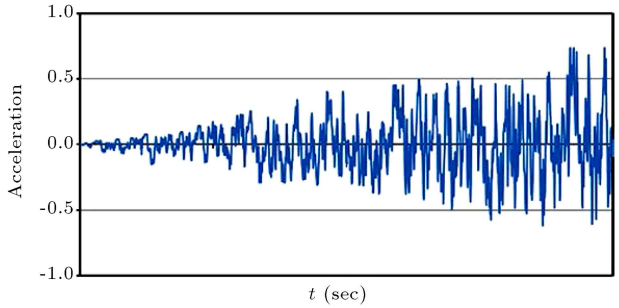

Figure 2. Typical ET accelerogram [5].

in Eq. (1)) corresponds to time [5].

$$\Omega(f(t)) = \text{Max}\left(\text{Abs}(f(t)) : \tau \in [0,t]\right), \tag{1}$$

where, Ω is maximum absolute operator; and $f(\tau)$ is the desired structural response history, such as inter-story drift ratio and base shear or other damage indices. To apply the ET method, the intensifying accelerograms are generated in such a way as to produce dynamic responses equal to those values induced by the desired response spectrum (such as the code design spectrum) at a predefined time (t_{Target}) [1,5]. Also, the results obtained by ET time history analysis can be compared with those of other analysis methods and, the performances of structures with different periods of free vibration can be compared. The first intensifying accelerograms suggested for ET had a linear intensification scheme. It means that the response spectrum of an ET accelerogram should be intensified proportionally with time. Hence, the target acceleration response of an ET accelerogram can be related to the codified design acceleration spectrum [5], as follows:

$$S_{\text{aT}}(T,t) = \frac{t}{t_{\text{Target}}} \times S_{\text{aC}}(T), \tag{2}$$

where, $S_{\text{aT}}(T,t)$ is the target acceleration response at time "t"; T is the period of free vibration; and $S_{\text{aC}}(T)$ is the codified design acceleration spectrum.

Using unconstrained optimization in the time domain, the problem was formulated as follows:

$$\min F(a_g) = \int_0^{T_{\max}} \int_0^{t_{\max}} \{\text{Abs}[S_a(T,t) - S_{\text{aT}}(T,t)]^2 + \alpha \text{Abs}[S_u(T,t) - S_{\text{uT}}(T,t)]^2\} dt.dT, \tag{3}$$

where, a_g is the ET accelerogram; $S_{\text{aT}}(T,t)$ is the target acceleration response; $S_{\text{uT}}(T,t)$ is the target displacement response at time t; $S_a(T,t)$ and $S_u(T,t)$ are the acceleration and displacement responses of the acceleration function at time t, respectively; and T is the period of free vibration. α is a relative weight parameter that can be used to adjust the effective penalty attributed to displacement deviations, as compared to acceleration deviations from target values. High values of α make the target function more sensitive to displacement response differences, and low values of α make the target function more sensitive to acceleration differences. Considering the theoretical correlation between the acceleration response and the relative displacement response, a high value of α should result in a better fit in the high period range, and a low value of α results in a better fit in the low period range. For different generations of the ET accelerograms, α may vary. For most ET generations, α has been set to 1.0, forcing a balanced penalty on either response parameter [1,2,5].

Based on the mentioned linear scheme, different sets of ET accelerograms can be generated in different ranges (linear or nonlinear), according to their compatibilities with different spectra. Each set consists of a group of intensifying acceleration functions (usually 3).

For example, three acceleration functions, named "ETA20f01-03" or, briefly, "f series", are created in such a way that the template response spectrum at $t = 10$ second matches the average response spectrum of major components of 7 real accelerograms (listed in FEMA440 for soil type C). In Figure 3, the response spectra of the f series are compared at different times. The spectral acceleration values corresponding to the target times of 5, 10 and 15 sec have been plotted in this figure. According to this figure, and, as expected from the ET concept, the values corresponding to 10 and 15 sec are twice and triple that of 5 sec, respectively [6].

3. Spectral characteristics of near fault earthquake

An earthquake is a shear dislocation that begins from a point on the fault and spreads with almost the same velocity of shear wave. In forward directivity, the fault rupture is propagated towards a site with very high velocity, producing high seismic energy. Propagation of the fault ruptures towards a site (forward directivity)

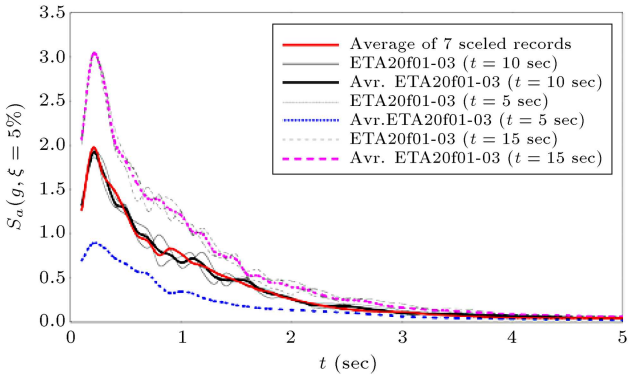

Figure 3. Response spectra of ETA20f01-03 at different times [6].

at very high velocity causes most of the seismic energy from the rupture to arrive in a single large long period pulse of motion, which occurs at the beginning of the record. It is oriented in the direction perpendicular to the fault, causing the strike-normal peak velocity to be larger than the strike-parallel peak velocity. Forward directivity results from the increasing of the response spectrum of the horizontal component normal to the fault strike at periods longer than 0.5 sec. This causes the peak response spectral acceleration of the strike-normal component to shift to longer periods; for example, from 0.25 seconds to as much as 0.75 seconds. Near fault effects cannot be adequately described by uniform scaling of a fixed response spectral shape. The increasing of spectral values is higher in the long periods as the earthquake magnitude increases. Figure 4 shows the effects of rupture directivity on the response spectrum of the Rinaldi record of the Northridge earthquake, 1994 [3].

Forward directivity effects are based on two conditions: 1) The rupture front is propagated towards the site; 2) The direction of slip on the fault is aligned with the site. The conditions for generating forward directivity effects are met mainly in the strike-slip faulting. Accordingly, the fault slip direction is oriented horizontally along the strike of the fault and the rupture is propagated horizontally along the strike, unilaterally or bilaterally. Backward directivity effects occur when the rupture is propagated away from the site. This fact results in the opposite effects of forward directivity, like long duration motions with low amplitudes at long periods. Forward directivity occurs in dip-slip faulting, including both reverse and normal faults as well [3].

Somerville et al. (1997) used a large set of near fault strong motion records to develop a quantitative model of rupture directivity effects. This model can be used to modify existing ground motion attenuation relations for incorporating directivity effects. The ground motion parameters, modified for directivity effects, are the average horizontal spectral acceleration and the ratio of strike-normal acceleration to strike-parallel acceleration. Strike-normal refers to the horizontal component of the motion normal to the fault strike. Strike-parallel refers to the horizontal component of the motion parallel to the fault strike [3].

In the Somerville's model, the amplitude variation due to rupture directivity depends on two geometrical parameters: 1) The smaller the angle between the directions of rupture propagation and the waves travelling from the fault to the site, the larger the amplitude; 2) The larger the fault rupture surface between the hypocenter and site, the larger the amplitude. The azimuth angle (θ) and length ratio (X) are considered for strike-slip, and the zenith angle (φ) and width ratio (Y) for dip-slip faults in the directivity model are presented in Figure 5. The effects of rupture directivity on ground motion amplitudes are modeled using the directivity functions, $X\cos(\theta)$, for strike-slip faults and $Y\cos(\varphi)$ for dip-slip faults. The dependency of the spectral amplification factor on $X\cos(\theta)$ and $Y\cos(\varphi)$ has been illustrated in Figure 6. These effects are started at the period of 0.6 sec and increase as the period increases [3].

Following the above model, the ratio of strike-normal to average horizontal of spectral acceleration depends on the magnitude, fault distance and directivity functions. The strike-normal motion is obtained through multiplying the attenuation relation value first by the average response spectral ratio, and, second, by the ratio of strike-normal to average horizontal. Strike-parallel spectral acceleration can be estimated using average horizontal and strike-normal components as well.

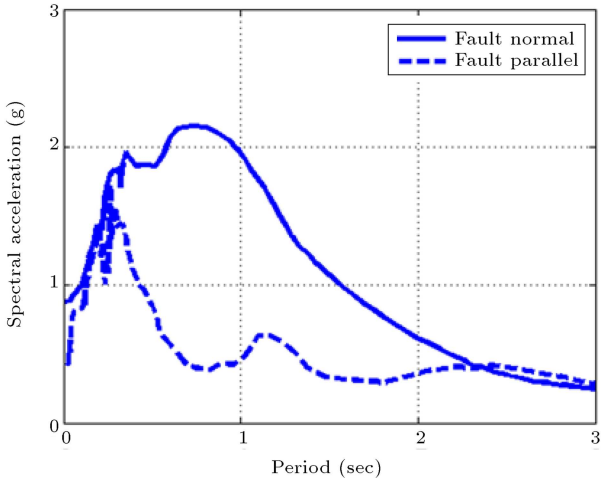

Figure 4. 5% damped response spectra for strike-normal and strike-parallel horizontal components of Rinaldi station [3].

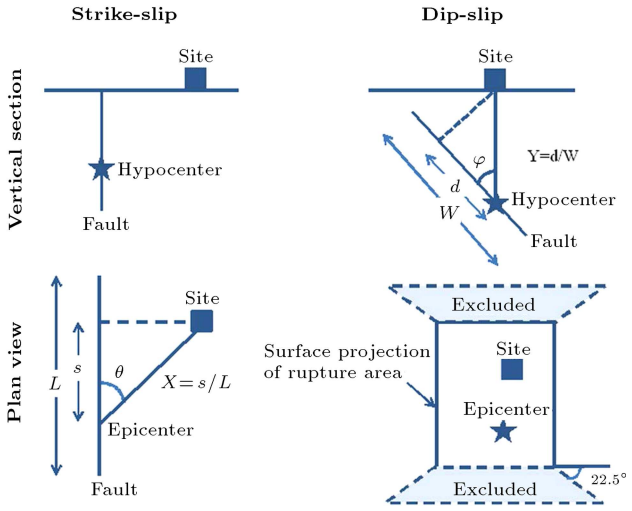

Figure 5. Rupture directivity parameters: θ and X for strike-slip faults; φ and Y for dip-slip faults [3].

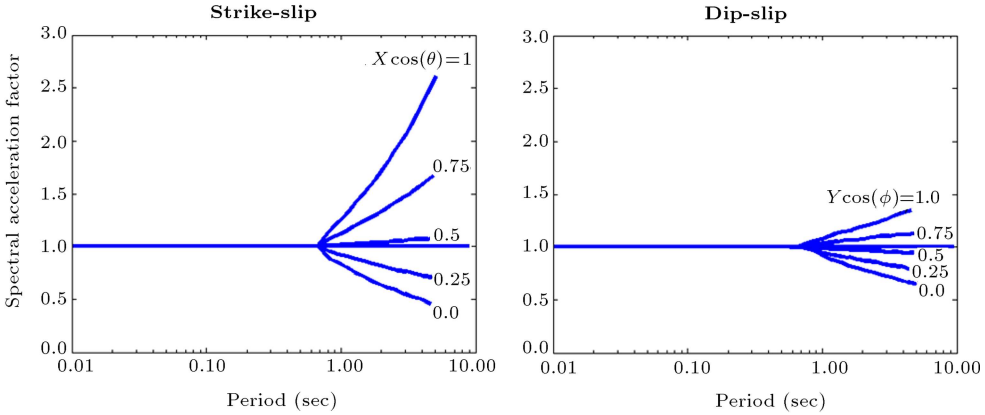

Figure 6. The dependency of response spectral factor on period and directivity function: $X\cos(\theta)$ for strike-slip faulting; $Y\cos(\varphi)$ for dip-slip [3].

In this research, the Abrahamson-Silva [4] attenuation relation has been used to generate the target spectra, modified by the Somerville directivity model and discussed in the following.

3.1. Abrahamson-Silva spectral attenuation relation

The general functional form of the relation is given as follows:

$$\ln\left(S_a(g)\right) = f_1(M_w, r_{\text{rup}}) + Ff_3(M_w) + \text{HW}f_4(M_w, r_{\text{rup}}) + Sf_5(\text{PGA}_{\text{rock}}), \quad (4)$$

where, $S_a(g)$ is spectral acceleration in g; M_w is moment magnitude; r_{rup} is the closest distance to the rupture plane in km; F is fault type; HW is a dummy variable for hanging wall sites; and S is a dummy variable for the site class [4].

3.2. Average horizontal response spectra

Average horizontal response spectra are obtained by multiplying $S_a(g)$ in Eq. (4) by Eq. (5) in the corresponding periods:

$$F_{\text{AH}} = e^y, \quad (5)$$

where:

$$y = C_1 + C_2 X\cos(\theta) \quad \text{for strike-slip} \quad M_w > 6,$$

$$y = C_1 + C_2 Y\cos(\varphi) \quad \text{for dip-slip} \quad M_w > 6.$$

X, Y, θ and φ are directivity parameters, shown in Figure 5; C_1 and C_2 are period dependent coefficients, clarified in Table 1, for both strike-slip and dip-slip faulting [3].

3.3. Ratio of strike-normal to average horizontal motions

The ratio of strike-normal to the average horizontal motion is expressed as follows:

$$\frac{\text{SN}}{\text{AH}} = e^{\frac{y}{2}}, \quad (6)$$

Table 1. The model's coefficients for spatial variation of average horizontal spectral acceleration [3].

	For strike-slip		For dip-slip	
Period	C_1	C_2	C_1	C_2
0.6	0	0	0	0
0.75	-0.084	0.185	-0.045	0.008
1	-0.192	0.423	-0.104	0.178
1.5	-0.344	0.759	-0.186	0.318
2	-0.452	0.998	-0.245	0.418
3	-0.605	1.333	-0.327	0.559
4	-0.713	1.571	-0.386	0.659
5	-0.797	1.757	-0.431	0.737

where:

$$y = C_1 + C_2\ln(r_{\text{rup}} + 1) + C_3(M_w - 6) \quad M_w > 6,$$

where, r_{rup} is the lowest distance from the rupture plane (here, assumed as 5 km); M_w is moment magnitude; and C_1, C_2 and C_3 are period dependent coefficients, listed in Table 2 [3].

The strike-normal spectral value is obtained by multiplying Eq. (6) to the modified average value of horizontal components achieved in Section 3.2. The values of horizontal components and strike-normal spectral values are manipulated in order to obtain the strike-parallel motion.

Figure 7 shows the procedure described for strike-slip faulting, with respect to $M_w = 7$ and deep soil.

4. Near fault acceleration function

For generating acceleration functions, the target times and spectra should primarily be specified. In this research, the acceleration function has been generated for both strike-slip and dip-slip faulting considering deep soil and shallow crustal soil, according to the Abramson-Silva assumption. Strike-normal, average horizontal and strike-parallel components have been

Table 2. The coefficients of the ratio of strike-normal to average horizontal spectrum [3].

Period	C_1	C_2	C_3
0.5	0	0	0
0.6	0.048	-0.012	0
0.7	0.079	-0.019	0
0.75	0.093	-0.022	0
0.8	0.108	-0.026	0
0.9	0.124	-0.03	0
1	0.139	-0.033	0
1.5	0.192	-0.046	0
2	0.231	-0.055	0.005
2.5	0.27	-0.065	0.011
3	0.304	-0.075	0.025
3.5	0.331	-0.084	0.046
4	0.351	-0.096	0.063
4.5	0.362	-0.098	0.081
5	0.369	-0.103	0.093

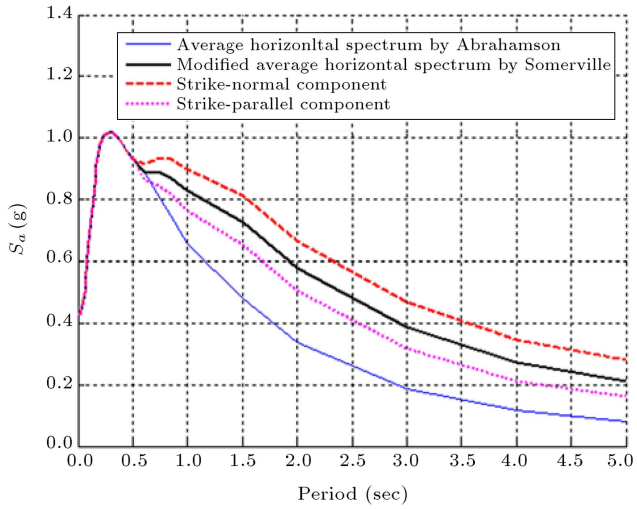

Figure 7. Near fault acceleration spectra considering strike-slip faulting, deep soil, $M_w = 7$ and $X\cos(\theta) = 1$.

considered in both cases of mentioned soils and focal mechanisms (dip-slip and strike-slip).

4.1. Target spectra

Here, target spectra are produced according to Section 3 for five moment magnitudes of 4, 5, 6, 7 and 8 in the 5 km distance from the rupture plane. Regarding the average horizontal component, five directivity conditions have been considered. Accordingly, $X\cos(\theta)$ and $Y\cos(\varphi)$ are set as 0, 0.25, 0.5, 0.75 and 1. To consider directivity effects on strike-normal and strike-parallel components, these values are set just as 0.5 and 1 to induce average and highest forward directivity conditions, respectively.

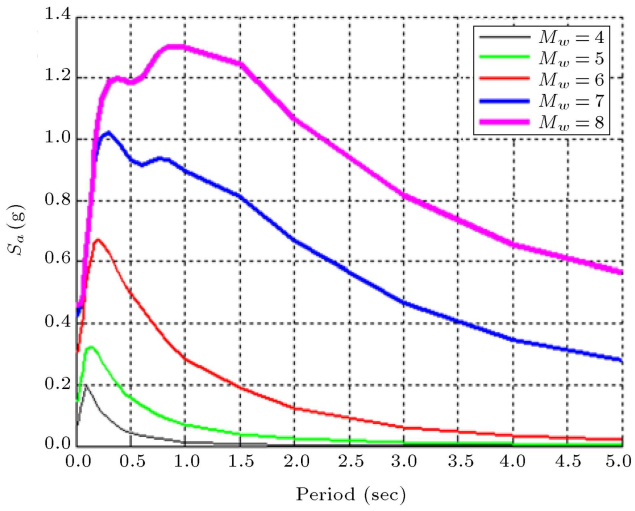

Figure 8. Spectral acceleration of strike-normal component in deep soil considering forward directivity for different magnitudes ($r_{\text{rup}} = 5$ km).

Figure 8 shows the target spectra of strike-normal components for deep soil and different magnitudes.

4.2. Target times

The most important spectral characteristics of ETAFs are target times and spectra. If the target time is set as $t = t_0$, then, ETAFs are calibrated in such a way that their response spectra in a window from $t = 0$ to $t = t_0$ match the design or codified spectrum with a unity scale. When the window of an acceleration function is from $t = 0$ to $t = K \times t_0$, its response spectrum is corresponded to K multiplied by the template spectrum at all periods. This characteristic is used to determine the target times for near fault acceleration functions.

$t = 10$ sec is assumed as the time at which the earthquake has the moment magnitude of M_w= 6. Therefore, this time and its corresponding target spectrum are considered as the bases. Target time for other moment magnitudes is approximately obtained as follows:

$$t_p(M_w) = \frac{S_a(M_w)_{T=1}}{S_a(6)_{T=1}} \times 10, \tag{7}$$

where, M_w is moment magnitude; $t_p(M_w)$ is target time corresponding to M_w; $S_a(M_w)_{T=1}$ is spectral amplitude corresponding to M_w at $T = 1$ sec; and $S_a(6)_{T=1}$ is spectral amplitude corresponding to $M_w = 6$ at $T = 1$ sec. Final target times are achieved based on engineering judgment of the above values. Target times and their corresponding moment magnitudes are listed in Table 3.

4.3. Generating the acceleration function

Near fault ETAFs has been generated based on a method used in the first generation of ET acceleration functions. Some deviations, generally minor for all

Table 3. Target times and their corresponding moment magnitudes.

Target time (sec)	Moment magnitude (M_w)
2	4
4	5
10	6
32	7
45	8

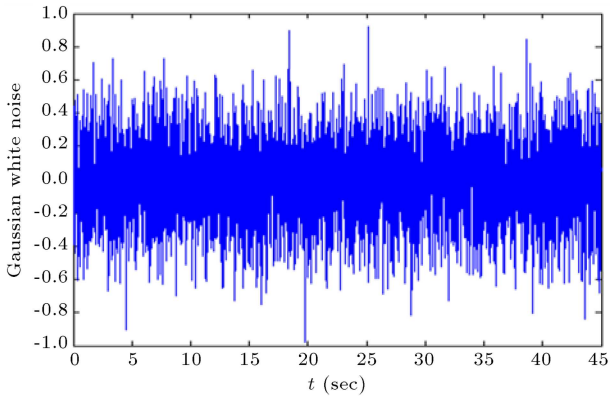

Figure 9. Gaussian white noise with time duration of $t = 45$ sec.

magnitudes, except for M=8, from the target spectra are accepted, while no optimization procedure for a perfect match has been used. First, a series of random numbers are produced having the Gaussian distribution of zero mean and the variance of unity with the time duration of the last target time (45 sec corresponded to magnitude 8), shown in Figure 9. The time step is set as 0.01 sec.

The frequency content of the above random numbers is then modified in order to resemble the accelerograms of real earthquakes. For this purpose, the filter functions, explained by Clough and Penzien [7], are applied to the random accelerograms as follows:

$$H_1(i\omega) = \frac{\left(1 + 2i\xi_1(\frac{\omega}{\omega_1})\right)}{(1 - \frac{\omega^2}{\omega_1^2}) + 2i\xi_1(\frac{\omega}{\omega_1})}, \quad (8)$$

$$H_2(i\omega) = \frac{\left(1 + 2i\xi_2(\frac{\omega}{\omega_2})\right)}{(1 - \frac{\omega^2}{\omega_2^2}) + 2i\xi_2(\frac{\omega}{\omega_2})}, \quad (9)$$

where, $\omega_1 = \frac{2\pi}{0.5}$, $\omega_2 = \frac{2\pi}{0.1}$ and $\xi_1 = \xi_2 = 0.2$ are used, such as the first generation of ETAFs [8]. It should be mentioned that frequencies higher than 25 Hz are filtered and neglected in this study. A sample frequency content resulted from the accelerogram of Figure 9 is plotted in Figure 10.

The acceleration whose frequency content has been modified is returned to the time domain with

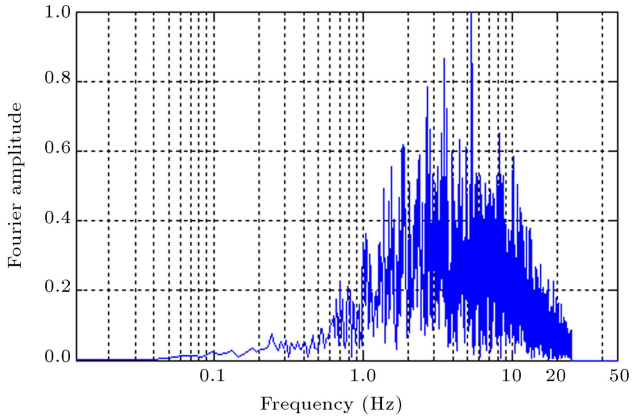

Figure 10. Modified frequency content resulted from the accelerogram shown in Figure 9.

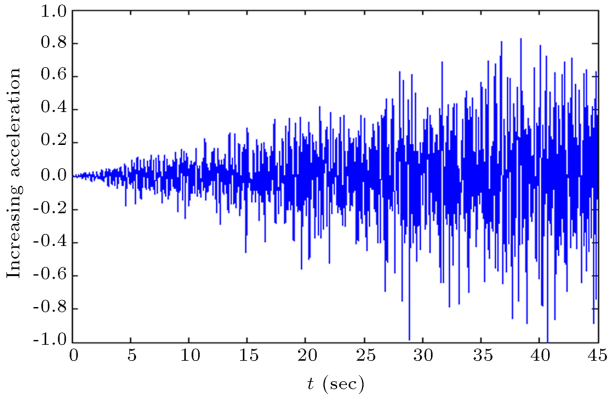

Figure 11. Intensifying acceleration.

inverse fast Fourier transformation. The resulted acceleration is multiplied by a profile function, $f(t) = \frac{t}{45}$, to take intensifying form, as shown in Figure 11.

Like conventional ETAFs, the resulted acceleration is modified in such a way that at some target times, the related response spectra are matched with their corresponding target spectra in the time window of 0 - target time. As mentioned before, five target times and spectra have been considered here; therefore, the process has 5 steps numbered by j. The target times (T_p) are defined as follows:

$$T_p = [2; 4; 10; 32; 45] \text{ sec.}$$

The acceleration presented in Figure 11 is multiplied by the window shown in Figure 12 to meet step j.

$T_p(j)$ is the jth target time, shown in Figure 12. The result will be 5 acceleration functions, whose values follow the initial acceleration function, shown in Figure 11, in the consecutive target times; their values are zero at other times. Fourier spectrum amplitude is modified for the resulted accelerations as follows:

$$A^{\text{new}}(i\omega)_j = A^{\text{old}}(i\omega)_j \times \frac{S_{aT}(\omega)_j}{S_a(\omega)_j}, \quad (10)$$

where, $A^{\text{old}}(i\omega)_j$ is the Fourier amplitude of the accel-

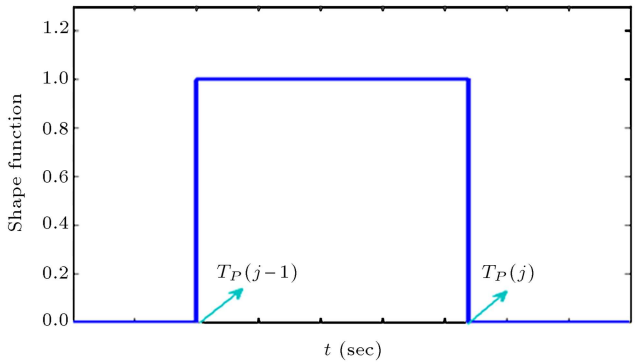

Figure 12. shape window for the jth step.

eration function of the jth step; $S_{aT}(\omega)_j$ is the jth target spectrum corresponding to 5% damping and $T_p(j)$, described in Sections 4.1 and 4.2; $S_a(\omega)_j$ is the 5% damped response spectrum of the acceleration function of the jth step; and $A^{\text{new}}(i\omega)_j$ is the modified Fourier amplitude of the acceleration function.

This process is repeated up to meet proper convergence between the response spectrum and the target spectrum. The above mentioned procedure is presented in Figure 13 for the 4th step as an example.

The final acceleration function is obtained by summing the accelerations resulted from the above mentioned method and shown in Figure 14. The record and its relevant spectra at different target times are depicted in this Figure.

Like conventional ETAFs, three acceleration functions have been generated for each case (different focal mechanisms, soil type and directivity condition) and the average value of results is used for analysis. The generated near fault acceleration functions and their abbreviations have been summarized in Table 4.

4.4. *Comparing new ETAFs with real accelerograms*

Every synthesized accelerogram should be able to satisfy some characteristics of real earthquakes. Although near fault earthquakes, which have further characteristics in addition to the directivity effect, rationally cannot be compared with new ETAFs, which

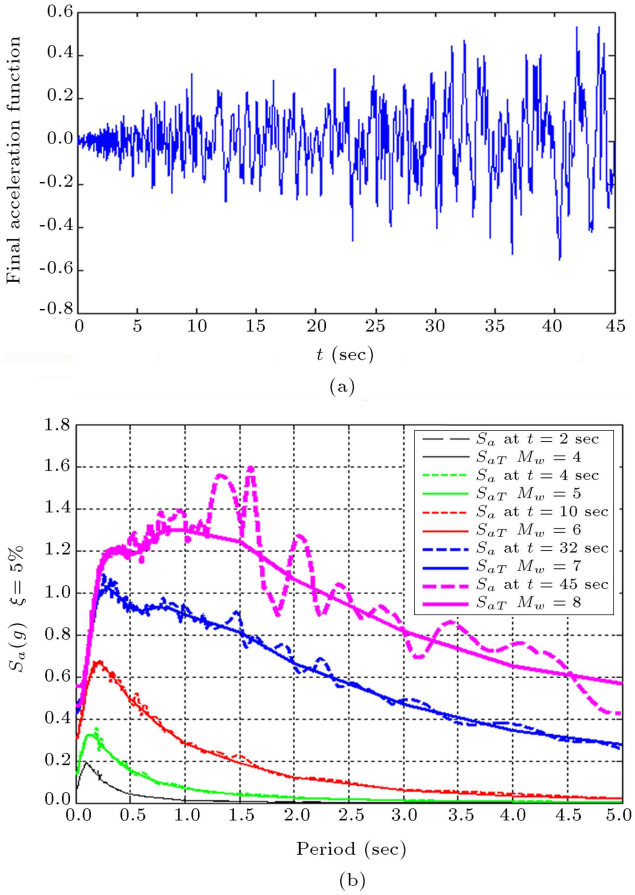

Figure 14. a) Generated ETAF. b) Response spectra at different target times.

model directivity effects only, some similarities can still be seen in several parameters such as the response spectrum, frequency content, power spectral density and Arias intensity. In this study, new acceleration functions are compared with real records selected only based on moment magnitude and distance from the rupture plane, as listed in Table 5, for both strike-slip and dip-slip faulting, and no directivity condition was considered in this selection. The records have magnitudes around 6 and are compared at $t = 10$ sec.

The acceleration response spectrum is one of

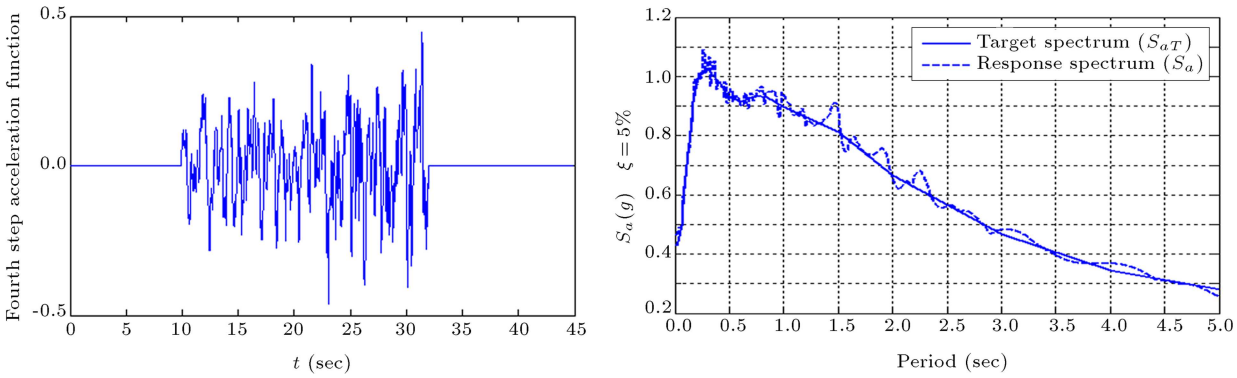

Figure 13. The procedure of new acceleration function generated for 4th step.

Table 4. The abbreviations of near fault acceleration functions.

Acceleration function type	Abbreviation
Strike-slip ET average horizontal component	SSETAH01-03
Strike-slip ET strike normal component	SSETSN01-03
Strike-slip ET strike parallel component	SSETSP01-03
Dip-slip ET average horizontal component	DSETAH01-03
Dip-slip ET strike normal component	DSETSN01-03
Dip-slip ET strike parallel component	DSETSP01-03

Table 5. Real earthquakes used in this study.

Station name	M_w	Mechanism	Component	R_{rup} (km)
Morganhill, Anderson dam	6.19	Strike-slip	Strike-normal	3.3
Morganhill, Hallsvalley	6.19	Strike-slip	Strike-normal	3.6
Morganhill, Coyotolake dam	6.19	Strike-slip	Strike-normal	0.5
ParkField, Cholame#8	6.19	Strike-slip	Strike-normal	12
NPS-cabazon	6.06	Dip-slip	Strike-normal	4
Desert hot springs	6.06	Dip-slip	Strike-normal	6.8
Palm spring airport	6.06	Dip-slip	Strike-normal	10

the most important parameters from an earthquake engineering point of view. The spectral acceleration of real records and ETAFs for both strike-slip and dip-slip faulting are plotted at $t = 10$ sec and shown in Figure 15(a) and (b). According to this figure, although the spectral values of near fault ETAFs and real records are different in some periods, they are significantly close to each other. The displacement and velocity of new ETAFs for the strike normal component of strike-slip faults are presented in Figure 15(c) and (d). The velocity and displacement values generally increase through time duration and do not reach zero at the end of the records. This phenomenon has also been observed for the ETAFs generated for far fault [9].

Dynamic responses of structures are very sensitive to the frequencies at which they are loaded. Earthquakes produce complicated loading, with components of motion that span a wide range of frequencies. The amplitudes of ground motions are distributed in different frequencies according to their contents [9]. The frequency content of ETAFs, related to the strike-normal component of the strike-slip fault, is compared with that of a real earthquake and presented in Figure 15(e). Based on the figure, the results of near fault ETAFs and real earthquakes are similar at almost the whole domain. The Intensity Arias (Ia) is closely related to the root mean square of acceleration, which is effective in characterizing the frequency content and power spectral density of accelerograms. According to Figure 15(f), the intensity Arias parameter matches the average ground motions for near fault ETAFs at $t = 10$ sec. Its value increases with a hyperbolic trend as the time increases, similar to conventional ETAFs [9].

5. The responses of SDOF systems

Here, three linear single degree of freedom systems with natural periods of 0.5, 1 and 1.5 sec have been considered to study the effects of directivity on the results of near fault ETAFs. Acceleration functions corresponding to the average horizontal component of three directivity conditions have been provided by setting three values of 0, 0.5 and 1 for the directivity parameter, $X\cos(\theta)$, and applied to the mentioned systems. In the ET method, the analysis results are usually presented by a curve in which the maximum absolute value of the damage measured in the time interval $[0; t]$ (as given in Eq.(1)) corresponds to time. Figure 16 shows the ET displacement curves. The rate of directivity effect on the responses increases as the periods of the systems and, also, the time, increase. According to Somerville, for producing near fault ETAFs, directivity affects responses beyond the structural period of 0.6 sec. This fact can be followed best in Figure 16. Regarding the system with a period of 0.5 sec, all site-source geometry conditions lead to the same results. It means that directivity has no effect on structural responses in this system. However, for the two other systems with periods of 1 and 1.5 sec, three directivity conditions affect the results after 10 sec. Moreover, the results for various directivity conditions in the system with period of 1.5 sec have more differences with each other compared to other systems, as expected.

Like conventional ETAFs, the equivalent time is used to compare analysis results of ET records with those of real records [10]. In this regard, the average

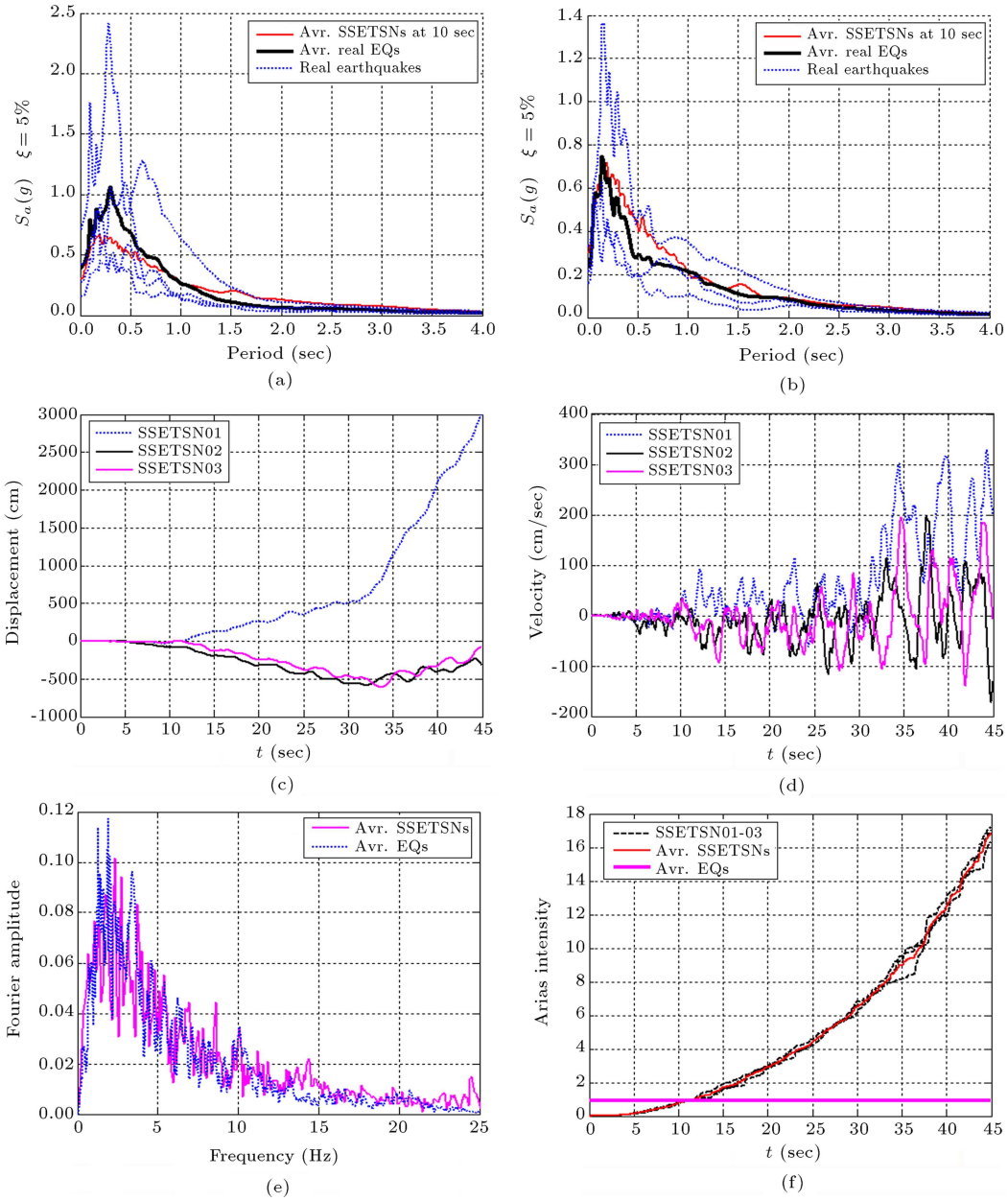

Figure 15. Comparing different parameters of near fault ETAFs and real earthquakes: (a) Comparison of new ETAFs and real earthquake response spectra for strike-slip faults; (b) comparison of new ETAFs and real earthquake response spectra for Dip-slip faults; (c) displacement of new ETAFs; (d) velocity of new ETAFs; (e) comparison of frequency content between new ETAFs (at 10 sec) and ground motions; and (f) Arias intensity for SSETSNs acceleration functions and ground motions.

value of the first-mode spectral acceleration ($S_{a,\text{Ave}}$) is calculated for real earthquake records.

Accordingly, the spectral acceleration of generated near fault ETAFs is calculated ($S_{a,\text{ET}}$) at the first-mode period of MDOF systems or the natural period of SDOF systems (T1) for the same level of those real earthquakes. Finally, the equivalent time is obtained by the following equation:

$$t_{\text{eq}} = \frac{S_{a,\text{Ave}}}{S_{a,\text{ET}}} \times T_P, \tag{11}$$

where, T_p is the target time corresponding to certain target spectrum. Target time is assumed as 10 sec to calculate the equivalent time, because the moment magnitude of real earthquakes is about 6. The results of the SSETSN set, introduced in Table 4, and the average of real earthquakes, listed in Table 5, have been calculated and compared for the SDOF system with a period of 1.5 sec and shown in Figure 17.

The displacement values of ET at 10 sec and those of real earthquakes are not the same, because: 1) Real earthquake spectrum and ETAF target spectrum have

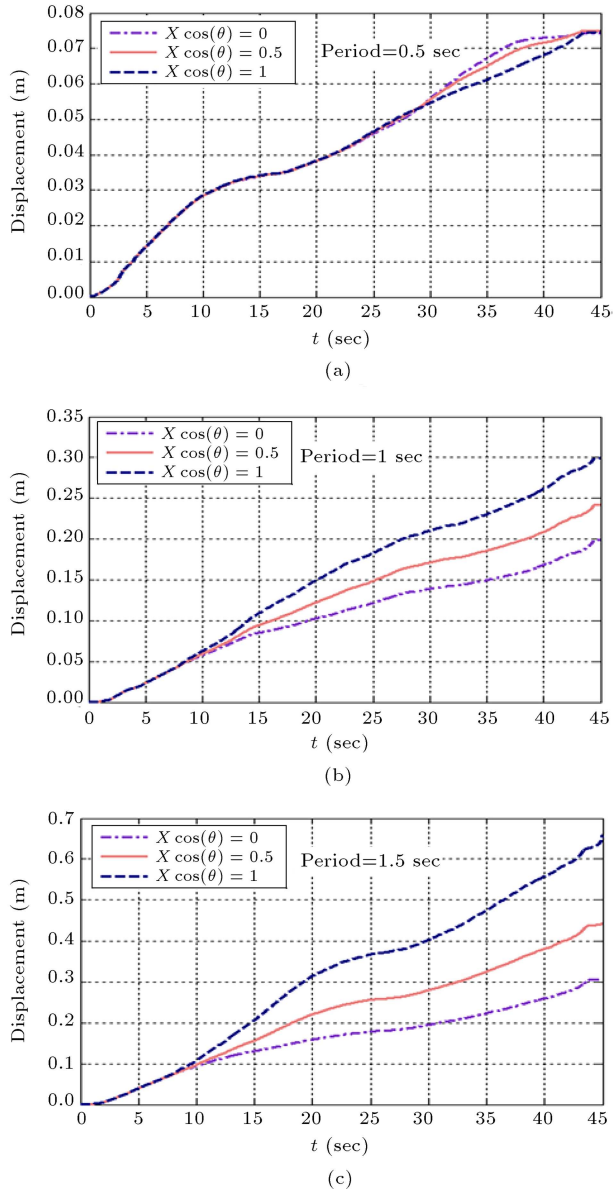

Figure 16. linear displacement responses under SSETAHs for different periods of SDOF systems.

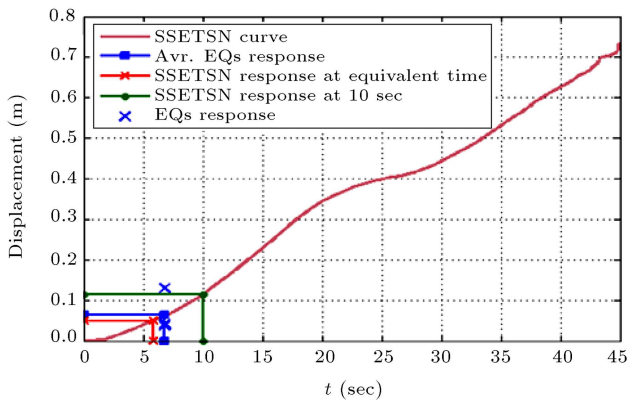

Figure 17. Comparing the linear displacement response of SSETSNs set and average of real earthquake for SDOF system with the period of 1.5 sec.

discrepancies, shown in Figure 15(a) and (b); 2) The ETAF spectrum is matched with the target spectrum at 5 points and has not enough accuracy to predict other spectral levels. Therefore, the ET result should be compared at the equivalent time. According to the figure, the results of these two methods become closer by using equivalent time.

6. The responses of MDOF systems

In this research, the responses of multi degree of freedom systems have also been studied under near fault ETAFs. For this purpose, 3 and 6 story steel braced frames with three bays have been used to verify the concept of the endurance time method. The SSETSNs series have been applied for time history analysis. These frames are designed according to the Iranian National Building Code (INBC), Section 10 [11], which is almost identical to AISC-ASD design recommendations [12]. The frames with various seismic resistance values have been categorized in 3 groups in order to compare their behavior, regarding the intensity levels of design lateral loads. These groups are: Standard, Under-designed and Over-designed frames; their names are ended with the letters S, W and O, respectively, listed in Table 6. As an example, an over-designed frame with 6 stories and 3 bays is abbreviated as "BF06B3O" in the mentioned table. Standard frames have been designed according to the base shear recommended by INBC for high seismicity areas in an equivalent static procedure [13]. Under-designed and over-designed frames have been designed based on one half and twice the codified base shear, respectively. The frames' masses are assumed equal in order to simplify the comparison. The geometry and section properties of the frames are presented in Figure 18, and some of their major characteristics in Table 6.

The nonlinear behaviors of the frames have been studied using a bilinear material model with a post-yield stiffness equal to 1% of the initial elastic stiffness. This material model is applied in the analysis using OPENSEES for beam, column and truss elements, with nonlinear distributed plasticity [14]. The dynamic soil-

Table 6. The specifications of frames.

Frames	Number of stories	Number of bays	Mass participation of mode 1	Period (sec)
BF03B3W	3	3	83.12%	0.46
BF03B3S	3	3	81.75%	0.4
BF03B3O	3	3	80.30%	0.33
BF06B3W	6	3	79.00%	0.96
BF06B3S	6	3	71.28%	0.73
BF06B3O	6	3	62.27%	0.64

structure interaction has been neglected, but the effects of $P-\Delta$ have been considered in the analysis.

6.1. ET analysis

ET analysis has been conducted on the frames subjected to the SSETSNs sets of acceleration functions.

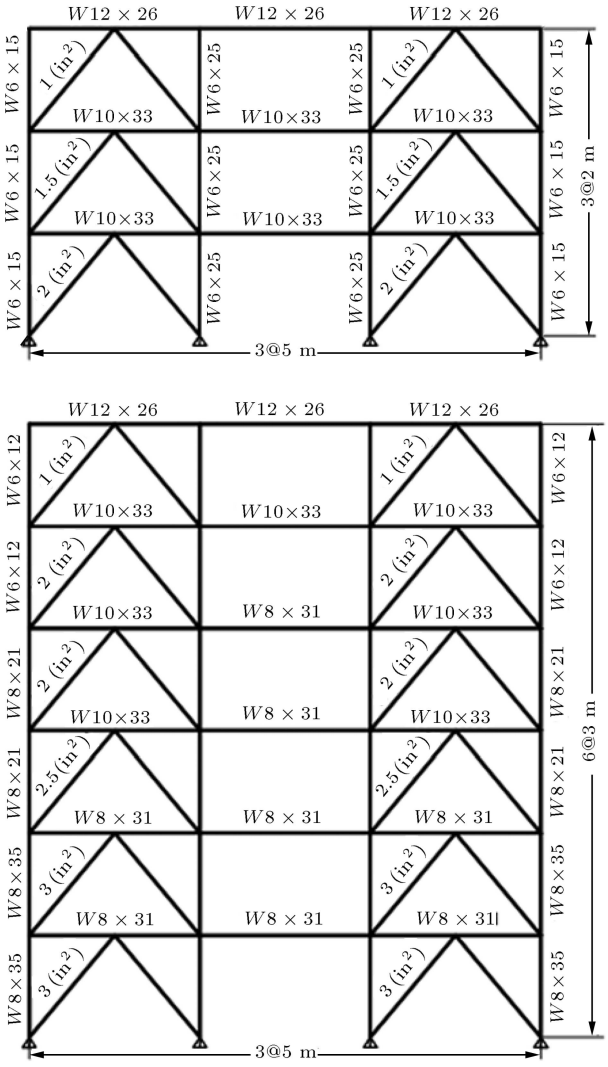

Figure 18. Schematics configurations of the frames used in this study.

ET analysis is like time-history analysis, except that in the former, the ground motions are replaced with acceleration functions. In this research, several damage indices, such as base shear, roof displacement and maximum story drift ratio, have been investigated. Figure 19 shows the base shear and roof displacement ET curves of the BF03B3S frames and their histories for near fault acceleration functions.

The rate of near fault effects has been studied on the responses of three and six story standard frames, and shown in Figure 20. Also, threshold times describing different earth quake levels have been marked. According to this figure, unlike the SDOF system, roof displacement ET curves, related to average and forward directivity conditions, do not diverge at the same time in the mentioned frames. The specifications of the BF03B3S frame with the natural period of 0.4 sec are summarized in Table 6. The directivity has no effect on this system at $t = 10$ sec, which is corresponded to $M_w = 6$. The curves' divergence points have been shifted to 22 sec, due to the nonlinear behavior. As time increases, the amplitude of excitation increases as well, and the frame experiences nonlinear status. The lateral stiffness value decreases, so the frame's period exceeds 0.6 sec. After this point, the responses are affected by directivity, according to the assumptions of this research, and shown in Figure 20(a). Regarding the BF06B3S frame, as the system's period is 0.73 sec (Table 6), directivity will affect the responses at 10 sec. The difference between the ET curves increases as the time increases; this is also seen in SDOF systems. According to the results obtained in this research, ETAFs can properly model the directivity effects. It should be mentioned that the forward and average directivity conditions are obtained in ETAFs production. In this regard, the values of 1 and 0.5 have been used for $X\cos(\theta)$ or $Y\cos(\varphi)$, respectively.

Figure 21 shows the different performances of a structure at different earthquake levels using the new ETAFs. Lower time is needed for the under-designed frame to meet the predefined damage index, compared to others, as it has a worthy performance.

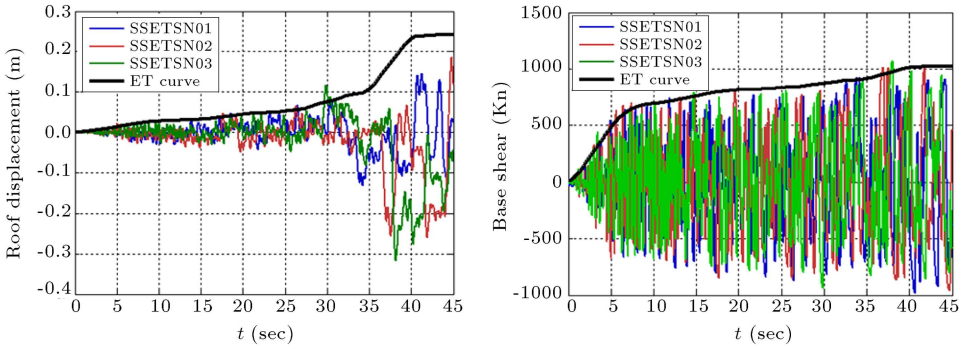

Figure 19. Generating ET curves from roof displacement and base shear histories of the BF03B3S frame considering forward directivity.

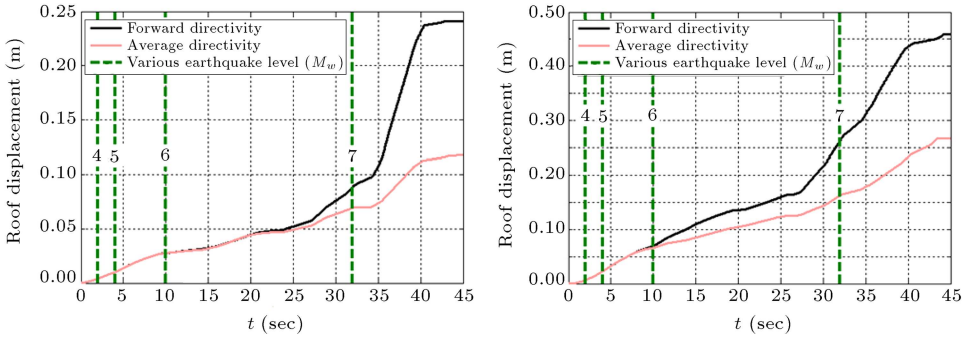

Figure 20. ET non-linear roof displacement curves of SSETSNs set: (a) BF03B3S; and (b) BF06B3S.

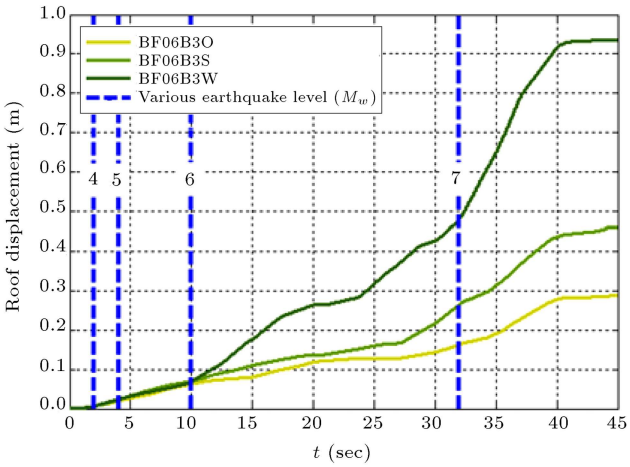

Figure 21. ET non-linear roof displacement curves of SSETSNs set for different alternatives of BF06B3 frames.

The over-designed frame has a higher endurance time and the best performance, regarding the same damage index. Therefore, the new ETAFs follow endurance time concepts well.

The maximum drift ratios, estimated by ET analysis under the SSETSNs set, and those of real records, at equivalent time, have been studied for both 3 and 6 story frames, and are shown in Figure 22. According to this figure, the results obtained by the two methods are not the same. However, analysis using the new ETAFs can predict the distribution pattern of drift ratio at different story levels. In general, the frames behave similarly under near-fault ETAFs and conventional ETAFs.

7. Conclusion

In this research, the ET method has been developed for near-fault regions. For this purpose, near fault target spectra have been used instead of conventional ET template spectrum. Such spectra have been provided through the Abramson-Silva attenuation relation and modified by Somerville coefficients. New sets of acceleration functions have been produced considering different components, soils and directivity conditions. SDOF and MDOF systems have been subjected to the new ETAFs and the obtained results are expressed as follows:

1. Unlike conventional ETAFs in which the spectra, corresponding to various earthquakes levels, have linear increasing relations for all periods uniformly, in the new ETAFs, establishing such relations is not reasonable due to the effects of directivity for higher periods on the near-fault regions.
2. Near-fault acceleration functions are produced with a progressed procedure compared to conventional ETAFs. The results show good convergence of the new ETAFs response spectrum with the target spectrum at target time. However, as the time increases, the rate of the mentioned convergence decreases. Moreover, new ETAFs have not enough

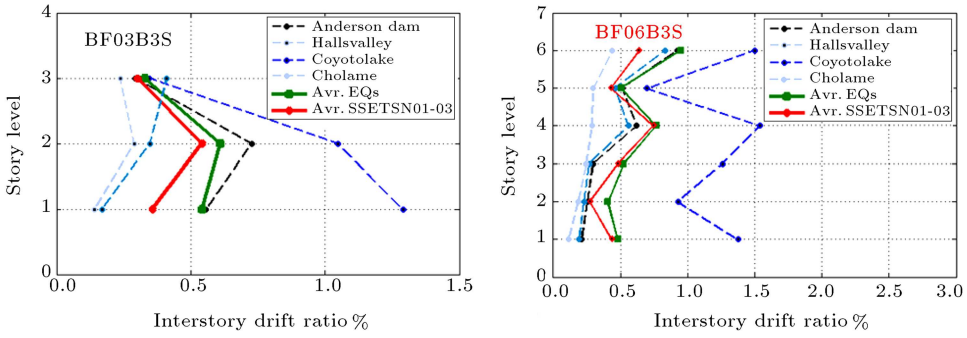

Figure 22. Distribution of maximum interstory drift ratios of BF03B3S and BF06B3S at different story levels obtained by ET at equivalent time and real earthquakes time history analysis.

accuracy to predict other spectral levels at the target time intervals.

3. Higher time intervals are needed in the applied method for matching the ETAF spectrum with a target spectrum related to high moment magnitude, such as 7 or 8, unless other optimization procedures are to be used.
4. In the new ETAFs, more parameters affect near-fault acceleration functions because of using attenuation relations. These parameters are the distance from the fault, focal mechanism, soil type and directivity conditions; so, new ETAFs may not have a widespread use for design purposes, unlike conventional ETAFs.
5. Like conventional ETAFs, the responses values obtained by the new ETAFs and real earthquakes are not the same; therefore, the equivalent time has been used for comparison. The results of the two methods become closer to each other at the equivalent time.
6. ETAFs response spectra are only matched with target spectrum at the target times defined in this study. However, the responses keep their intensifying forms in ET curves. Therefore, the results will be valid for other moment magnitudes as well.
7. Studying SDOF systems shows that the directivity effects can properly be modeled by the new acceleration function. As expected, the directivity conditions have no effect on the linear systems with periods of less than 0.6 sec. However, high period systems have different responses under various strike components and directivity conditions. This variety increases as the time increases.
8. Studying nonlinear MDOF systems proves how new ETAFs can follow its basic concepts. Regarding nonlinear systems with a period of less than 0.6 sec, the frame's lateral stiffness decreases as the time increases, due to its nonlinear behavior. Then, the responses are affected by directivity, as the frame's period exceeds 0.6 sec Concerning under-designed, standard and over-designed frames, new ETAFs follow the endurance time concept properly.

Acknowledgments

The authors would like to thank Khajeh Nasir Toosi University of Technology for supporting this research effectively.

References

1. Estekanchi, H.E., Valamanesh, V. and Vafai, A. "Application of endurance time method in linear seismic analysis", *Engineering Structures*, **29**(10), pp. 2551-2562 (2007).
2. Riahi, H.T. and Estekanchi, H.E. "Seismic assessment of steel frames with endurance time method", *Journal of Constructional Steel Research*, **66**(6), pp. 780-792 (2010).
3. Somerville, P., Smith, N., Graves, R. and Abrahamson, N. "Modification of empirical strong ground motion attenuation relations to include amplitude and duration effects of rupture directivity", *Seismological Research Letters*, **68**(1), pp. 180-203 (1997).
4. Abrahamson, N.A. and Silva, W.J. "Empirical response spectral attenuation relations for shallow crustal earthquakes", *Seismological Research Letters*, **68**, pp. 94-127 (1997).
5. Mirzaee, A., Estekanchi, H.E. and Vafai, A. "Application of endurance time method in performance-based design of steel moment frames", *Scientia Iranica*, **17**(6), pp. 482-492 (2010).
6. Riahi, H.T. and Estekanchi, H.E. "Application of ET method for estimation of inelastic deformation demands of steel frames", *8th International Congress on Civil Engineering*, Shiraz University, Shiraz, Iran, May 11-13 (2009).
7. Clough, R.W. and Penzien, J., *Dynamic of Structure*, McGraw-Hill Inc, USA (1993).
8. Estekanchi, H.E., Vafai A. and Sadeghazar, M. "Endurance time method for seismic analysis and design of structure", *Scientia Iranica*, **11**(4), pp. 361-370 (2004).
9. Valamanesh, V., Estekanchi, H.E. and Vafai, A. "Characteristics of second generation endurance time acceleration functions", *Scientia Iranica*, **17**(1), pp. 53-61 (2010).
10. Riahi, H.T., Estekanchi, H.E. and Vafai, A. "Estimates of average inelastic deformation demands for regular steel frames by the endurance time method", *Scientia Iranica*, **16**(5), pp. 388-402 (2009).
11. MHUD. "Iranian national building code, part 10, steel structure design", Ministry of Housing and Urban Development, Tehran, Iran (2006).
12. American Institute of Steel, *Allowable Stress Design Manual of Steel Construction*, 9th Ed. Chicago: AISC (1989).
13. BHRC "Iranian code of practice for seismic resistant design of buildings", standard no. 2800-05, 3rd Ed., Building and Housing Research Center, Tehran, Iran (2005).
14. OpenSees "Open system for earthquake engineering simulation", Pacific Earthquake Engineering Research Center (2002). http://peer.berkeley.edu/

Biographies

Behzad Ghahramanpoor Soomaie obtained his BS in degree Structural Engineering from the Department

of Civil Engineering at Tabriz University, Iran, in 2010, and his MS degree from Khajeh Nasir Toosi University of Technology, Iran, in 2012. His MS thesis was conducted under the supervision of Dr. Nader Fanaie. His field of research includes artificial accelerograms, seismic behavior of steel structure and near fault effects. He has published 3 conference papers up to now.

Nader Fanaie obtained his BS, MS and PhD degrees in Civil Engineering from the Department of Civil Engineering at Sharif University of Technology, Tehran, Iran. He graduated in 2008 and, at present, is a faculty member of Khajeh Nasir Toosi University of Technology, Tehran, Iran. He has supervised 7 MS theses up to now. His field of research includes seismic hazard analysis, earthquake simulation, seismic design and IDA. He has published 15 journal and conference papers, and also 10 books. He received 3rd place in the first mathematical competition, held at Sharif University of Technology, in 1996, and a Gold Medal in "The 4th Iranian Civil Engineering Scientific Olympiad" in 1999. In 2001, he achieved the first rank in the exam and obtained a PhD scholarship abroad, and was acknowledged as an innovative engineer on 'Engineering Day', in 2008.

Hussein Jahankhah obtained his BS, MS and PhD degrees in Civil Engineering from the Department of Civil Engineering at Sharif University of Technology, Tehran, Iran. He graduated in 2010 and, at present, is a faculty member of the the International Institute of Earthquake Engineering and Seismology in Iran. His field of research includes soil-structure interaction and near fault earthquakes, in which areas he has published 6 journal papers.